Journal of Colloid and Interface Science 563 (2020) 281–290

Contents lists available at ScienceDirect

Journal of Colloid and Interface Science

journal homepage: www.elsevier.com/locate/jcis

Interfacial rheology and relaxation behavior of adsorption layers of the triterpenoid saponin Escin

Gerard Giménez-Ribes, Mehdi Habibi, Leonard M.C. Sagis *

Physics and Physical Chemistry of Foods, Wageningen University, Bornse Weilanden 9, 6708WG Wageningen, the Netherlands

GRAPHICAL ABSTRACT

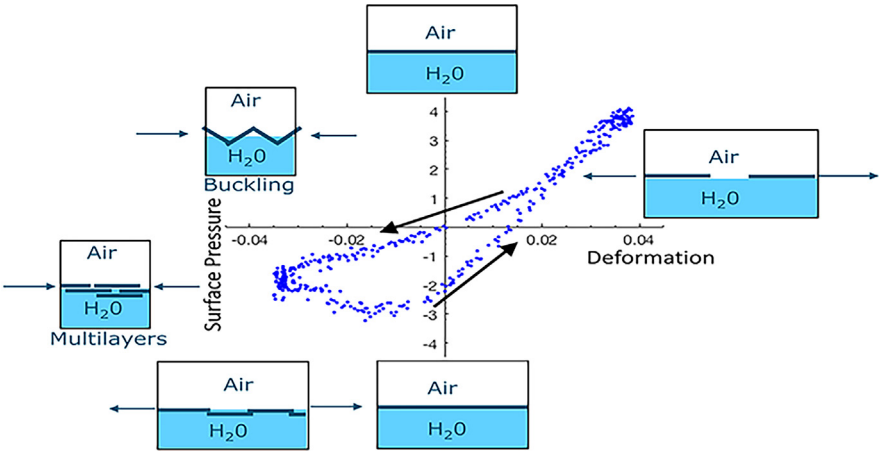

ARTICLE INFO

Article history:
Received 20 September 2019
Revised 12 December 2019
Accepted 13 December 2019
Available online 18 December 2019

Keywords:
Escin
Saponin
Dilatational
Shear
Relaxation
Interfacial rheology
Stretched exponential
Non-linear Viscoelastic (NLVE) regime

ABSTRACT

Hypothesis: Escin, a monodesmosidic triterpenoid saponin, was shown previously to form viscoelastic interfaces with a very high dilatational and surface shear storage modulus. This is expected to be due to the arrangement of Escin into 2D disordered soft viscoelastic solid interfacial structures, which results in turn in a distribution of relaxation times.

Experiments: The responses to dilatational and surface shear deformations of Escin-stabilized air-water interfaces were studied, both in the linear viscoelastic (LVE) and non-linear (NLVE) regime. Step relaxation and amplitude sweeps were performed in dilatation experiments. For surface shear, amplitude sweeps and creep recovery experiments were performed.

Findings: Escin stabilized-interfaces displayed a highly non-linear behavior in dilatation as seen in the Lissajous plots. In large oscillatory shear the Lissajous curves had a rhomboidal shape, indicating intracycle yielding and recovery, typical of glassy systems. The relaxation of the interface showed stretched exponential behavior, with stretched exponents typical of disordered solids with dynamic heterogeneity.

Abbreviations: LVE, Linear Viscoelastic; NLVE, Nonlinear Viscoelastic; LMWS, Low Molecular Weight Surfactants; FT, Fourier-transform; SAOSS, Small Amplitude Oscillatory Surface Shear; LAOSS, Large Amplitude Oscillatory Surface Shear; SAOD, Small Amplitude Oscillatory Dilatation; LAOD, Large Amplitude Oscillatory Dilatation; PAT, Profile Analysis Tensiometer; DWRG, Double Wall Ring Geometry; MD, Molecular Dynamics; CV, Compound-Voigt.

* Corresponding author.
E-mail address: leonard.sagis@wur.nl (L.M.C. Sagis).

https://doi.org/10.1016/j.jcis.2019.12.053

The use of surface rheological measurements beyond the commonly measured LVE regime clearly has provided new insights into the behavior of these interfaces and their microstructure. These results highlight the need to reconsider other complex interfaces as disordered solids and not as 2D homogenous viscoelastic fluids.

1. Introduction

Saponins, like Escin, have previously been studied mainly for their pharmacological uses. For instance, Escin is a candidate compound for developing anti-leukemia drugs based on its ability to induce apoptosis in leukemia cells [1]. It has been applied in chemo-prevention and treatment of colon cancer [2], and has also been extensively studied for its anti-inflammatory properties [3,4]. Only recently more attention has been paid to the interfacial behavior of Escin [5].

Saponins are a class of plant based molecules which present surface activity due to their amphiphilic structure. The basic structure of a saponin consists of a hydrophobic part, aglycone, with one or more sugar residues attached via glycosidic bonds. Based on the type of aglycone, saponins can be classified into steroids or triterpenoids. Escin is a monodesmosidic (one sugar chain attached to the aglycone) triterpenoid saponin [5], which was previously shown to impart very high surface shear and dilatational viscoelastic moduli to interfaces [6–8]. It has a molecular weight (1131.269 g mol^{-1}) similar to that of low molecular weight surfactants (LMWS) such as Tween 20 (1225 g mol^{-1}), and much smaller than other surface active biomolecules (e.g. proteins), which also show interfacial viscoelasticity. Therefore, it forms a viscoelastic interface faster than proteins do.

LMWS do not generally self-assemble into more complex two dimensional interfacial microstructures, after adsorption to an interface, and therefore the surface dilatational properties of interfaces stabilized by these components are mainly governed by the exchange of the LMWS between interface and bulk as explained in the Lucassen-van den Tempel model [9,10]. When surface active species are present that can self-assemble into interfacial structures such as 2D gels or soft glasses, the interfacial dynamics will be characterized by much higher surface shear and dilatational storage moduli, and lower surface loss tangents, compared to LMWS stabilized interfaces [11,12]. The high values for the surface shear and dilatational moduli observed for Escin-stabilized interfaces are an indication that this molecule self-assembles into solid-like structures, after adsorption to the interface.

The dilatational modulus quantifies the response of an interface to an all-sided area change, in either compression or expansion. It is the equivalent in two dimensions of the 3D bulk modulus. The complex dilatational modulus E_d^* is defined as [13]:

$$E_d^* = \left(\frac{\Delta\gamma}{\Delta A/A_0}\right) = E' + iE'' \tag{1}$$

for low amplitude harmonic deformations of angular frequency ω, where ΔA is the amplitude of the area oscillation, $\Delta\gamma$ is the amplitude of the surface tension oscillation and A_0 the equilibrium surface area. E_d^* is a complex number where the real part E' accounts for the dilatational elasticity or storage modulus, and the imaginary part $E'' = \omega\eta_d$ for the dilatational viscosity or loss modulus [14]. When subjecting the interface to sinusoidal oscillations in the linear response regime (small amplitudes), the surface tension will oscillate with the same frequency as the area, but with a phase shift, δ. Similarly, the surface shear modulus G^* can be measured using small amplitude oscillation of the in-plane shear stress and strain (and phase shift between them), and calculated with [15]:

$$G^* = |G^*|(\cos\delta + i\sin\delta) = G' + iG'' \tag{2}$$

where G' is the surface shear storage or elastic modulus, and G'' is the surface shear loss or viscous modulus.

Both E_d^* and G^* are obtained by applying a Fourier transformation on the oscillatory surface pressure (dilatational deformation) or surface stress (shear deformation). If the deformation is in the linear viscoelastic (LVE) regime, the signal will generate only a first or fundamental harmonic, of which the phase shift and intensity are used to calculate the modulus. But if the deformations enter the nonlinear regime, higher harmonics will appear in the frequency spectrum, and both E_d^* and G^* cease to be meaningful measures for the response of the interface [16,17]. For exploring these non-linearities in interfacial rheology several methods have been applied before, such as the use of Fourier-transform (FT) rheology [18–20] or the decomposition of the stress response into Chebyshev polynomials [21]. More recently, the use of Lissajous-Bowditch plots (from hereon referred to as Lissajous plots) based on the works of [16] for bulk rheology have also been introduced for dilatational [12,15,22–27] and shear [15,28] deformations of the interface. Lissajous plots can be created for surface shear experiments by plotting the stress signal versus the strain or shear rate, and for dilatational rheology by plotting the surface tension (or alternatively surface pressure) versus deformation [11].

A quantitative analysis of the Lissajous plots was suggested by Ewoldt et al. [16], by calculating the stiffening factor, S, according to $S = (G'_L - G'_M)/G'_L$ and the thickening factor, T, defined as $T = (\eta'_L - \eta'_M)/\eta'_L$. Here, G'_L and G'_M are the large-strain elastic modulus and minimum-strain elastic modulus, respectively. The viscosities η'_L and η'_M are the large-rate dynamic viscosity and the minimum-rate dynamic viscosity, respectively. Both the S and T factors are dimensionless, with $S > 0$ indicating strain stiffening, $S = 0$ indicating a linear elastic response, $S < 0$ implies strain softening, $T > 0$ indicates shear thickening, $T = 0$ implies linear viscous behavior, and $T < 0$ indicates shear softening behavior. This way of analyzing the Lissajous plots allows for the study of intracycle elastic (S factor) and viscous (T factor) non-linearities. Similarly, Van Kempen et al. [22] defined the strain-stiffening rations in extention (S_{ext}) and compression (S_{com}) for dilatational experiments. The study of non-linear behavior better reflects many processes in biological (e.g. mastication) or in industrial processing (e.g. handling and transportation) where deformations go well beyond the LVE regime [29–32]. The Lissajous plots provide information about the strain softening/hardening and strain rate thinning/thickening behavior, which provides clues on the actual microstructure of the interface, both near and far from equilibrium. Besides oscillatory deformations, interfaces can also be tested in step dilatational strain and surface shear creep experiments, to gain information on the relaxation behavior of the surface microstructure. For example, by subjecting interfaces to step expansion/compression, previous studies have shown that some viscoelastic interfaces show dynamic heterogeneity, and apparently have a soft disordered solid-like structure [33].

The aim of this study was to study the interfacial rheology of Escin-stabilized air/water interfaces, both within the LVE and NLVE regime, in surface shear and in dilatational mode. Escin-stabilized interfaces were studied with small and large oscillatory surface shear tests (SAOSS and LAOSS), and small and large oscillatory dilatation (SAOD and LAOD). The large amplitude measurements were analyzed using Lissajous curves. Studies of the behavior of interfaces in the NLVE regime are still scarce in literature, and to the best of our knowledge, this is the first study to carry out a thorough analysis of saponin-stabilized interfaces beyond the LVE regime. The interfaces were also subjected to large step dilatational measurements, and surface shear creep-recovery tests. These test were performed to probe the relaxation behavior of the interfaces. Our results provide novel insight on the behavior of these interfaces, in a regime which is highly relevant for applications, but has not been studied in detail before. Our results confirm the structure suggested for Escin-stabilized interfaces, proposed based on experiments [6,34] and molecular dynamics simulations [8,35], and provide new insight on the microstructure of these molecules at the interface.

2. Materials and methods

2.1. Materials

Escin was purchased from Sigma-Aldrich Co., Missouri, (Escin with ⩾95% purity, product No. E1378). Solutions were prepared in ultrapure water (MilliQ Purelab Ultra, Germany).

2.2. Surface rheology measurements

2.2.1. Surface Dilatational rheology

For the determination of the surface tension of the air/water interface of Escin solutions (5 g L^{-1} in phosphate buffer 10 mM at pH 7), a profile analysis tensiometer PAT (Sinterface, Berlin, Germany) was used. Amplitude sweeps were performed at frequencies of 0.001 Hz, 0.005 Hz, 0.01 Hz, 0.02 Hz, 0.05 Hz and 0.1 Hz, for amplitudes ranging from 3.5% to 7%. From the oscillation signals, Lissajous curves were constructed by plotting the surface pressure, $\Pi(t) = \gamma(t) - \gamma_0$ versus the deformation, $(A(t) - A_0)/A_0$, as done by van Kempen et al. [22]. All experiments were performed after an equilibration time of 2400 s at 20 °C, using a pendant drop with an equilibrium area of 20 mm^2, suspended from a 1.99 mm capillary.

Stress-relaxation experiments were performed with a fast compression or expansion of the drop (3.5%, 5% and 10% area) after 2400 s of equilibration, followed by a relaxation of 2000 s. The relaxation curve was fitted to a combination of a stretched and a regular exponential function [33]:

$$\gamma(t) = a\, exp^{\left(\frac{-\Delta t}{\tau_1}\right)^{\beta}} + b\, exp^{\left(\frac{-\Delta t}{\tau_2}\right)} + l \qquad (3)$$

where β is the stretch exponent ($0 \leqslant \beta \leqslant 1$), a and b are constants, τ_1 and τ_2 are the characteristic times that account for relaxation and aging, respectively, and l is the asymptotic surface tension value reached after relaxation. The curve fitting tool available in Matlab was used to obtain these parameters. The parameters obtained are averages of 6 independent measurements.

2.2.2. Surface shear rheology

The surface shear measurements of the air/water interface of the Escin solutions (5 g L^{-1} in phosphate buffer 10 mM at pH 7) were performed using a AR-G2 rotational rheometer (TA Instruments, DE, USA). A double wall ring geometry (DWRG) was used, which consists of a circular channel which is filled with 18.8 mL of sample. A Pt/Ir alloy ring with a diamond shape cross-section is then placed at the air-water interface. Amplitude sweeps were performed at frequencies of 0.1 Hz and 1 Hz for strains from 0.01 to 40%. Lissajous curves were constructed by plotting the stress, σ, against the strain, ε, or the shear rate, $\dot{\varepsilon}$, for one of the repetitions at each frequency. Creep-recovery experiments were performed with different stresses (0.209 mN m^{-1}, 0.52 mN m^{-1} and 1.5 mN m^{-1}) for a given creep time t_{CR} of 150 s, and recovery was monitored for 1000 s. All experiments were performed after an equilibration time of 2400 s at 20 °C. The circular channel and ring were rinsed with MilliQ water and ethanol before each analysis, and the ring was flamed to ensure any organic contamination was removed.

3. Results and discussion

3.1. Surface rheology of Escin

3.1.1. Surface dilatational rheology

In the amplitude sweeps with the PAT, we varied the amplitude in the range between 3 and 7%. Higher deformations could not be applied, since at amplitudes above 7% the deformations of the droplet interface became strongly non-affine, i.e. deformations in the neck region of the droplet deviated significantly from those in the apex region, and the droplet shape could no longer be fitted by the Young-Laplace equation with sufficient accuracy. In the range of amplitudes we tested the fitting error was at most 2%. For higher amplitudes, a different analysis technique would have to be used, referred to as capillary meniscus dynamometry [36], in which both droplet shape and droplet pressure are used to analyze non-affinely deformed droplets.

The raw data obtained from an amplitude sweep performed at 0.01 Hz is presented in Fig. 1a, with the oscillation corresponding to 5% deformation shown in detail in Fig. 1b. From the significant degree of asymmetry in Fig. 1b one can already see the strong non-linear behavior. The response deviates significantly from a simple sinusoidal response, which would have given a perfectly symmetric ellipsoidal plot. We observed higher harmonics in the response for all amplitudes and frequencies studied (The relative intensity of the second, third and fourth harmonic for the oscillations at 0.01 Hz are provided as supplementary material). Using only the first harmonic of the Fourier transform of the surface pressure to calculate E_d^*, as the software of the PAT does, would then give unrealistic results [11]. For this reason we chose to plot the results in the form of Lissajous curves, as seen before in Van Kempen et al. [22]. For constructing the Lissajous plot (Fig. 1c), the initial and final oscillation cycles were left out. The arrows in this plot indicate which part of cycle the segments of the plot correspond to. For example, the arrow pointing to the left denotes compression, and the arrow pointing to the right denotes expansion.

From the Lissajous curve one can observe an unusual behavior of this interface which arises upon compression. The compression part of the cycle in Fig. 1c runs from +0.04 to −0.04 (upper arrow in the plot). At a strain of about +0.02, the curve crosses the expansion part of the loop, and subsequently the slope of the plots levels off, indicating strain softening. For larger deformation amplitudes, the crossover becomes even more noticeable (see Fig. 2). After maximum compression is reached (about −0.04), and the expansion part of the cycle begins, the surface pressure continues to decrease, until the strain is approximately equal to 0. After that the surface pressure starts to increase in an almost linear fashion. The rest of the Lissajous curves, corresponding to amplitudes sweeps performed at 0.02, 0.05 and 0.1 Hz are provided as supplementary material.

The assembly of saponins into 2D clusters was first proposed by Golemanov et al. [34], and the same authors also proposed this

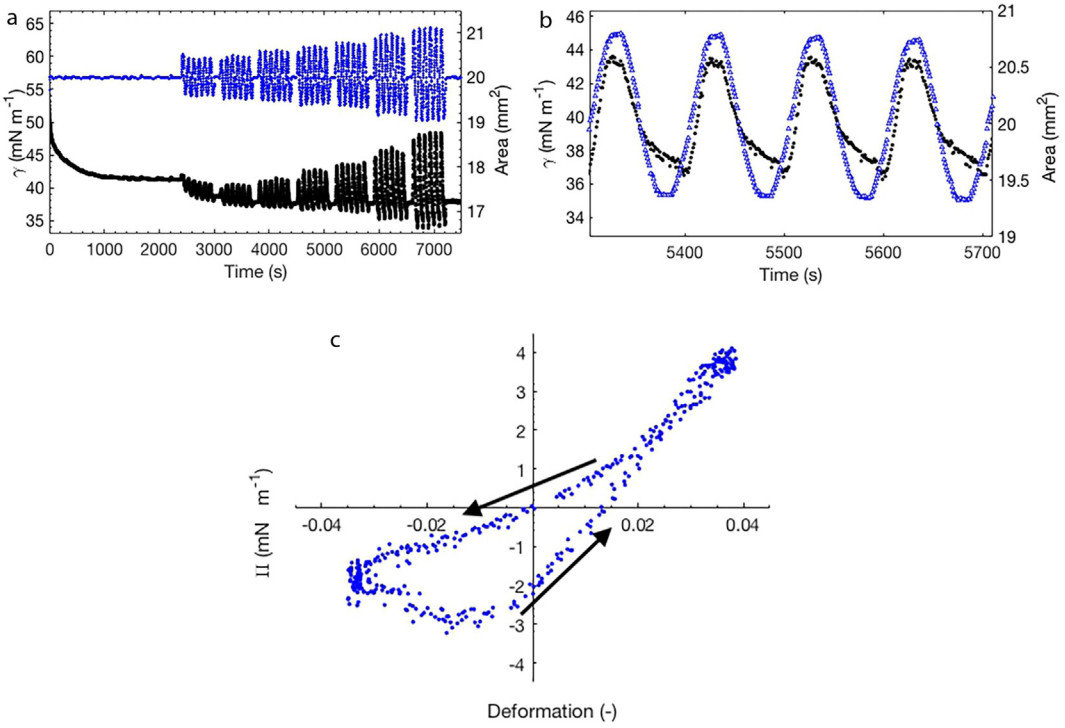

Fig. 1. (a) Amplitude sweep performed at 0.01 Hz with amplitudes of 3%, 3.5%, 4%, 4.5%, 5%, 6%, and 7% area deformation (b) Augmented image of the oscillation at 5% deformation. Blue dots correspond to the area oscillation, and black dots to the surface tension. (c) Lissajous plot corresponding to 5% amplitude area oscillation at 100 s period.

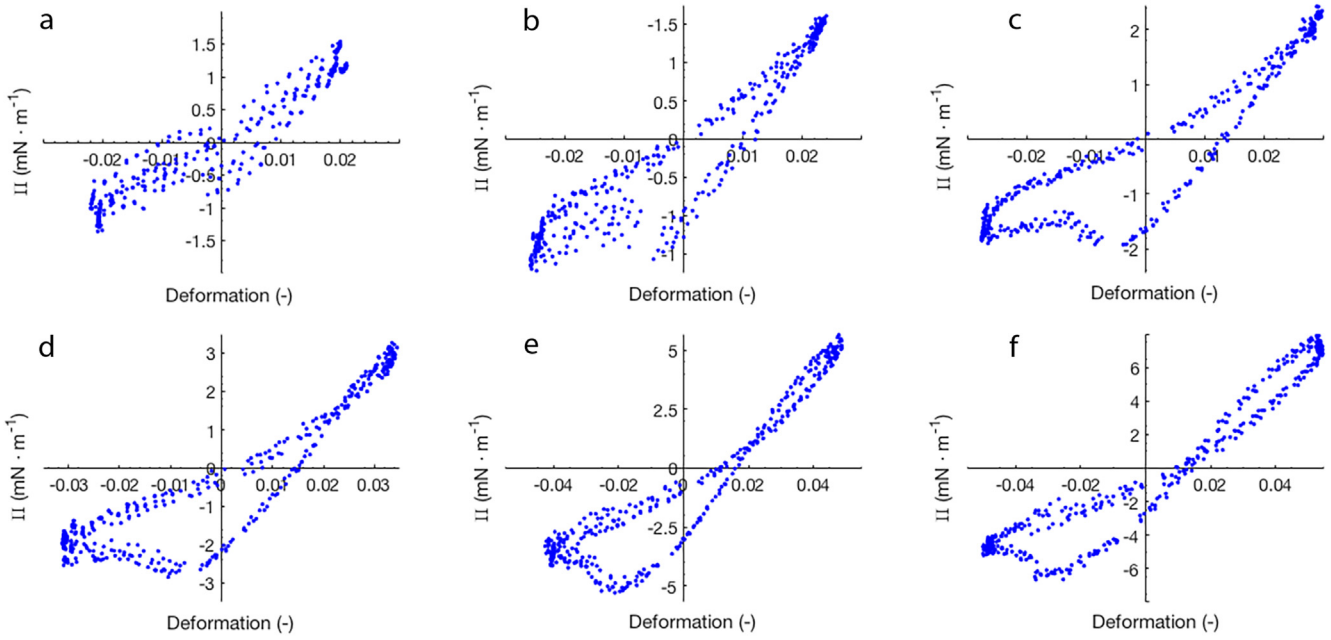

Fig. 2. Lissajous plots obtained from amplitude sweep performed at 0.01 Hz (Fig. 1a). Amplitudes: (a) 3%, (b) 3.5%, (c) 4% , (d) 4.5%, (e) 6.%, and (f) 7%.

behavior for Escin [6]. More recently, Tsibranska et al. [8] studied the assembly of Escin at air/water interfaces by performing atomistic molecular dynamics (MD) simulations, and their results provide clear insight on the origin of the unusual behavior of these interfaces in LAOD experiments. Their results showed how Escin molecules self-assemble rapidly on *ns* timescales into 2D surface clusters, after adsorption to the interface, due to long-range attractive van der Waals forces between the aglycone part of the molecule, and intermediate dipole-dipole and short-range H-bonds between the sugar moeities of the molecule. Tsibranska et al. [8] estimated an interaction of ~10 kT between the aglycone parts, and a total of ~7 kT distributed between H-bonds occurring within the sugar moieties, adding up to a total of ~17 kT of interaction. This implies that the Escin molecules are strongly bound in the clusters, and that these will have significant rigidity. When an interface with adsorbed rigid 2D clusters is compressed, the cluster

density will increase until a maximum surface packing fraction is reached, and the interface is in a jammed state. It was recently shown by the same authors that at a denser packing, the number of intermolecular H-bonds increase, rather than forming more H-bonds with water (which would result in desorption to the bulk) [35]. Upon further compression several phenomena can occur: (1) clusters are pushed out of the interface into the adjoining aqueous phase, (2) clusters slide over each other, forming multilayer structures, or (3) the structures remain at the interface and the interface starts to buckle. In view of the strong interactions between the Escin molecules, the latter two scenarios are likely more predominant, although the first one cannot be completely excluded.

With this in mind, our experimental LAOD results suggest that upon compression, the packing density of rigid clusters increases until buckling occurs or multilayers form. We did not observe the typical wrinkles and ridges that form on the interface associated with buckling. Such patterns were observed only for larger deformations and even then they were only transient, as we will discuss later. Hence, multilayer formation is a more likely explanation than buckling. The latter is responsible for the softening behavior we observe as the degree of compression increases. Upon expansion, the structure is stretched again, and during this phase the surface pressure is either nearly constant or even decreases a bit. To understand how this can lead to a decrease in surface pressure, we must realize that for complex interfaces of this kind, the parameter that we extract from the PAT measurements is not a real surface tension. It is an effective surface stress which apart from the surface tension includes contributions from deviatoric stresses. In the early phase of the expansion, clusters may be sliding over each other, and the friction involved in this gives an additional contribution to the surface stress, leading to a decrease in the surface pressure. Most likely, in this phase the structure is converted back to a mono-layer. Once the deformation is close to zero, further expansion starts to separate the clusters, breaking the attractive forces such as H-bonds, after which the surface pressure rapidly increases. At this point when the surface pressure is at a maximum, some adsorption of new Escin molecules might occur. However this adsorption will be limited, since Escin is expected to have a barrier-controlled adsorption as seen for *Quillaja* saponins [37]. It should be noted that all Lissajous plots shown have been shifted upward and centered, since the oscillations did not occur around the value of γ_0 achieved before the start of the oscillations.

Amplitude sweeps were performed as well at frequencies of 0.001 Hz and 0.005 Hz, but a downward baseline shift of both the area and surface tension was observed, being much more pronounced for 0.001 Hz (Provided as Supplementary Material). This made it impossible to plot Lissajous curves with the data. A possible explanation for this shift is that using oscillation periods of 200 s (0.005 Hz) or 1000 s (0.001 Hz) may allow for enough reorganization of the molecules within an oscillation cycle, by either in-plane diffusion or exchange between interface and bulk-phase. As mentioned before, the effects of mass transfer on the response cannot be completely excluded for this relatively small molecule.

To analyze the relaxation behavior of the molecules at the interface, after applying a step compression or expansion, the results were fitted with a combination of a stretched exponential and a regular exponential function (Eq. (3)). Surprisingly, after compression, the surface tension did not increase back to the equilibrium value, showing even a slight further decrease after compression for some of the repetitions, similar to the baseline shift seen in the Lissajous plots. An example compression curve is shown in the Supplementary Material. The fact that we do not see any relaxation of the surface tension after compression, gives again a strong indication that the solid-like 2D clusters upon compression slide over each other to form multilayers. As a result of the strong interactions between the molecules, these structures do not show any relaxation in the time scale of the experiment, neither by in-plane rearrangement, nor desorption. That the latter does not occur was also proposed by [7], based on compression experiments in Langmuir troughs. With the aid of a high speed camera we could observe the formation of wrinkles at the interface when subjecting the drop to a fast and large compression (Fig. 3), which indicates that initially the interface did buckle upon compression. But after the appearance of these wrinkles, if the compression is further increased, the wrinkles suddenly disappear. When the interface is compressed even further, the wrinkles start forming again (a video corresponding to the image is provided in the Supplementary Material). This suggest that after buckling, the stress that builds up in the interface is partially released by sliding of the clusters over each other. When this structure is further compressed it jams again, and starts to buckle again. These intermittent buckling events of the interface further indicate the limited desorption that occurs of Escin back into the bulk, due to the high surface binding energy [38]. The formation of wrinkles has been observed before for hydrophobin proteins [39,40], *Acacia* gum [41], asphaltenes [42,43], AFD4 and AM1 peptides [44], and saponins [37,45]. It is important to note that we do not observe relaxation of the surface tension back to equilibrium in compressions up to 10%. But the relaxation that we observe with the high speed camera after buckling, could in principle also be due to ejection of Escin clusters back to the bulk at some critical coverage value, and therefore we cannot completely exclude this scenario at larger compression. In the present study we will only analyze quantitatively the relaxation after different expansion amplitudes (Table 1).

The data shows an agreement with the fit of $R^2 \geqslant 0.983$ for all repetitions. A β value of 1 would indicate relaxation with only one single timescale. A value of $0 < \beta < 1$ indicates dynamic heterogeneity, which means there are local variations in the relaxation kinetics on the surface [46]. In our case, $\beta \approx 0.48$, and this value is not affected by the step amplitude in the range of step sizes we applied. These values show agreement with those reported in [33] of 0.4–0.6 for expansion of other complex interfaces, such as those stabilized by proteins, protein aggregates, particles, or polymers. The dynamic heterogeneity observed here suggests that

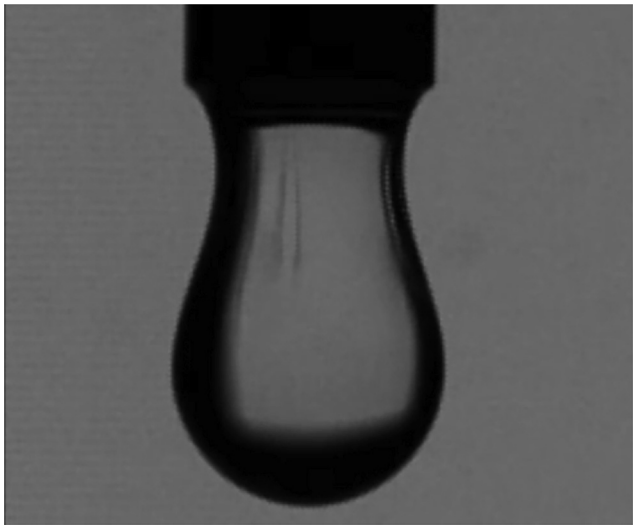

Fig. 3. Image showing the presence of wrinkles at the interface for large compression, as seen with the high speed camera. The outer diameter of the capillary corresponds to 1.75 mm.

Table 1
Rheological parameters obtained from fitting Eq. (3) for the relaxation stage after applying different amplitude of expansion (%).

Parameter	3.5%	5%	10%
a (mN m^{-1})	6.8 ± 1.4	8.4 ± 1.1	9.0 ± 1.9
b (mN m^{-1})	1.8 ± 0.5	1.9 ± 0.3	1.6 ± 0.2
l (mN m^{-1})	44.9 ± 1.9	46.1 ± 1.1	46.6 ± 1.1
β	0.49 ± 0.05	0.48 ± 0.04	0.48 ± 0.04
τ_1 (s)	10.9 ± 2.9	12.4 ± 3.6	10.7 ± 3.3
τ_2 (s)	1327.6 ± 220.5	1306.2 ± 677.2	1080.0 ± 423.5

upon expansion, the interface is broken down into clusters or domains with a wide distribution of sizes, which rearrange themselves over time at the interface, at different rates. The presence of these domains would imply weaker regions, where the fracture and yielding of the interface occur (explained below in the surface shear experiments). The characteristic times for relaxation, τ_1, and aging, τ_2, show that the interface has a relaxation which is two orders of magnitude smaller than the time for aging rearrangements. The asymptotic value for surface tension at equilibrium after relaxation, represented by the l parameter, increases for higher deformation amplitudes with respect to γ_{eq}. Probably, for larger expansions the interfacial structures are more disrupted, and the increase in l would mean that the previously more ordered packing is not recovered by relaxation (Fig. 4).

3.1.2. Surface shear rheology

From the shear strain sweeps, Lissajous plots were constructed for both shear stress versus strain and shear stress versus shear rate, for different selected strains. The results are shown in Fig. 5a–e for stress-strain Lissajous plots (stress-shear rate Lissajous plots provided as Supplementary Meterial). At small strain ε, Escin shows a response which is predominantly elastic, with $G' \sim 1100$ mN m^{-1} and $G'' \sim 60$ mN m^{-1} respectively, at 0.02% strain amplitude and 1 Hz, which results in an almost straight line for the Lissajous curve (data not shown). As the strain is increased, the Lissajous curve starts to become more ellipsoidal (Fig. 5b). The transition from a line to an ellipse is the result of a change in magnitude and phase angle of the fundamental harmonic. However, for Lissajous curves at strain $\geqslant$0.83% the shape starts to deviate from that of an ellipse as can be seen in Fig. 5c for 0.98% strain, indicating the presence of higher harmonics in the oscillating stress response [47]. At larger oscillation strains, the Lissajous plot exhibits a rhomboidal shape (Fig. 5d), which has previously been attributed to glassy systems [48], for which the stress after yielding is nearly independent of the strain (leading to the near horizontal parts of the loop). This behavior is different for gels, which exhibit a stress overshoot after yielding, leading to a local minimum in that part of the cycle [49]. This indicates that the structure of the interface belongs to the category of 2D jammed systems, and is not a 2D gel. The rhomboidal shape indicates, starting from the lower left corner of the loop, that the structure initially gives a predominantly elastic response, until the stress equals the yield stress, after which the structure breaks down and the interface begins to flow. When the strain approaches its maximum positive value (upper right corner of the plot) the shear rate decreases to zero, and the structure (partially) recovers, showing again first an elastic response and then yielding as the oscillation proceeds in the opposite direction. For the oscillations performed at 1 Hz and strains $\geqslant$ 15%, superimposed oscillations appear in the plateau region of the Lissajous plot (Fig. 5e). This phenomenon was related before to the effects of inertia [50], and therefore its relation to interfacial behavior is not discussed here.

In some of the Lissajous plots at strains around 1% we observed discontinuities inside an oscillation cycle (Fig. 6). By plotting the maximum σ obtained from the plots (i.e. the stress amplitude) as function of the strain, we could confirm the fracturing of the interface occurring at strain values $\sim$ 1% (Fig. 7).The maximum σ shows a clear fracture point, after which σ suddenly decreases.

A quantitative analysis of the Lissajous plots was performed and the results are presented in Fig. (8). The S factor agrees with the strain sweeps presented before, being close to zero (linear behavior) for both frequencies up to 0.8% strain for 1 Hz and 1% for 0.1 Hz. Surprisingly, above these strain values the interfaces exhibit intracycle strain stiffening, according to the S factor. But at strains of $\geqslant$ 1.8%, the T factor shows strong intracycle shear thinning behaviour, and this dominates the overall response, which is hence shear thinning [51]. This apparent strain stiffening in the elastic response was previously addressed by Mermet-Guyennet et al. [47]: for large deformations, after the interfacial structure yields, the tangent modulus G'_M, defined as $G'_M = (d\sigma/d\varepsilon)|_{\varepsilon=0}$has a value near zero. The secant modulus, which corresponds to $G'_L = (\sigma/\varepsilon)|_{\varepsilon=\varepsilon_0}$ will then determine the S factor with $G'_M \to 0$, resulting in values close to 1, which can be interpreted erroneously as strain stiffening. The missing bar at 20% strain in Fig. 8a is due to the superimposed oscillations mentioned before, and hence the slope at zero strain is not representative of G'_M. In Fig. 8b, the missing bars at small strains (0.1 Hz) are due to too low shear rates, resulting in Lissajous plots with too much noise to allow for a sufficiently accurate analysis.

We performed creep-recovery experiments by applying small stresses (0.209 mN m^{-1}, 0.52 mN m^{-1} and 1.5 mN m^{-1}, which were all found to be in the linear regime) for a creep time of 150 s. The data was fitted with the Compound-Voigt model (CV) used before by Golemanov et al. [34] for saponins. It consists of one Maxwell element and two Kelvin-Voigt elements positioned sequentially. A schematic representation can be found in [34]. Using this model, the compliance under creep will follow

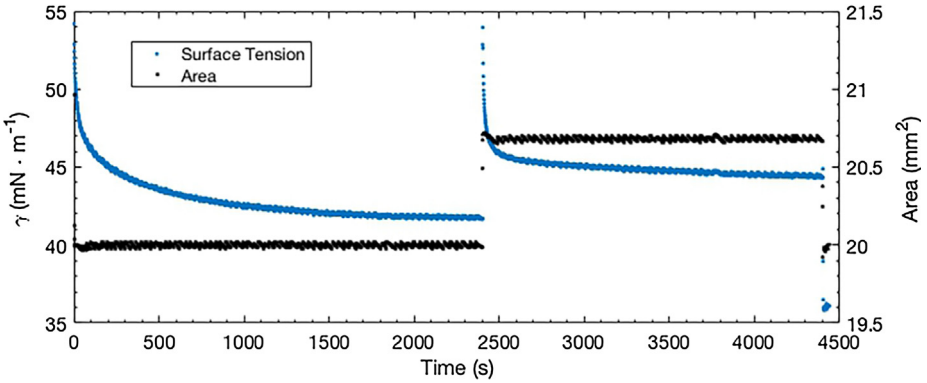

Fig. 4. Stress-relaxation experiment performed at 3.5% area expansion. The relaxation was studied over 2000 s.

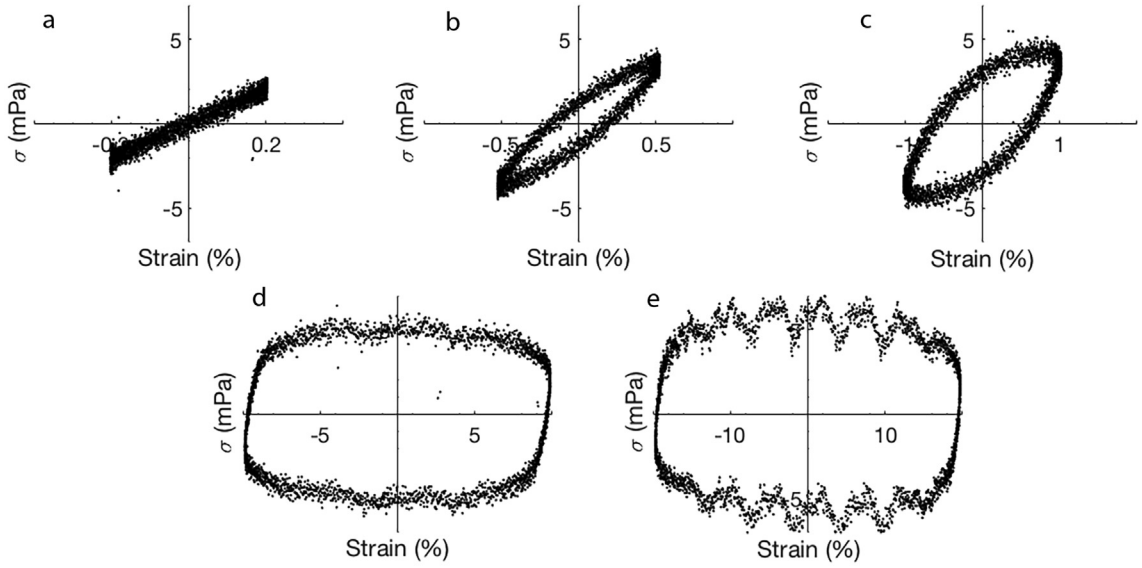

Fig. 5. Stress as a function of strain (elastic) Lissajous curves are constructed at strain of (a) 0.2% , (b) 0.52% , (c) 0.98%, (d) 10.47%, and (e) 20.69%. Strain sweeps performed from 0.01% to 40% strain at 1 Hz. Averages and standard deviation calculated from three measurements.

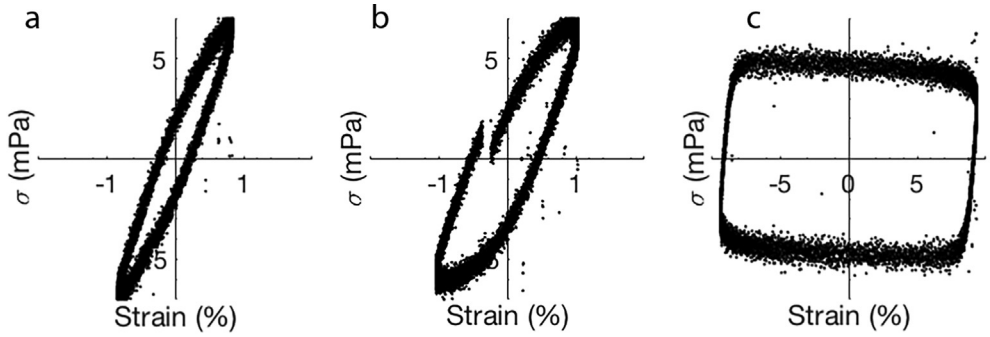

Fig. 6. Lissajous plots constructed from strain sweep at 0.1 Hz showing the higher stress achieved before fracture at a strain of 0.83% (a), the discontinuities inside an oscillation cycle at 0.97% (b) and the lower stress after fracture at 10.44% (c). All Lissajous have the same *y*-axis values (−7 to 7 mPa).

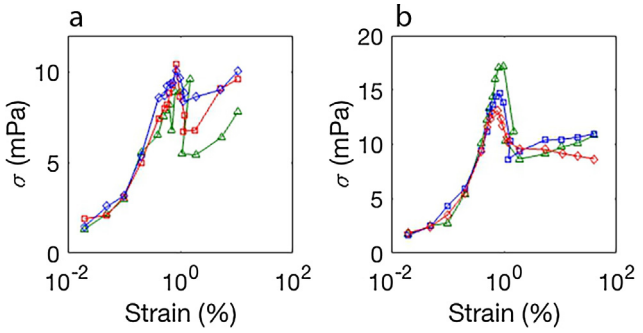

Fig. 7. Maximum stress observed from the Lissajous plots at different strains during the strain sweeps at 1 Hz (a) and 0.1 Hz (b), where the three repetitions are shown independently. Lines are guide to the eye.

$$J_C(t) = \frac{1}{G_0} + \frac{1}{G_1}\left[1 - \exp\left(-\frac{t}{\lambda_1}\right)\right] + \frac{1}{G_2}\left[1 - \exp\left(-\frac{t}{\lambda_2}\right)\right] + \frac{t}{\eta_0} \quad (4)$$

and under recovery,

$$J_R(t) = \frac{t_{CR}}{\eta_0} + \frac{1}{G_1}\left[1 - \exp\left(-\frac{t}{\lambda_1}\right)\right]\exp\left(-\frac{t-t_{CR}}{\lambda_1}\right) + \frac{1}{G_2}\left[1 - \exp\left(-\frac{t}{\lambda_2}\right)\right]\exp\left(-\frac{t-t_{CR}}{\lambda_2}\right) \quad (5)$$

where G_0, G_1 and G_2 are the elasticities of the Maxwel spring, and Kelvin springs 1 and 2, respectively, η_0 is the viscous response of the Maxwell dashpot, and λ_1, λ_2 are the relaxation times of the Kelvin elements 1 and 2, respectively.

The remaining parameters of the CV model can be calculated by $\eta_i = G_i\,\lambda_i$ and $\lambda_0 = \eta_0/G_0$. The fitting parameters were obtained by fitting both equations simultaneously to the experimental data (Table 2). G_0 corresponds to the initial instantaneous elastic response, determined from the compliance ($J_i = 1/G_i$). The value of 1.09 N m^{-1} is consistent with the G' observed in the linear region during the strain sweeps. We obtained a remarkably high viscous response from the Maxwell dashpot analogue (η_0). This high value is not surprising, considering that in the linear regime Escin behaves as a soft solid at the interface, with a fracture stresses ranging from ∼ 8 mPa to ∼ 17 mPa. (A fit of the parameters shown in Table 2 to the averaged experimental data from the three stresses is presented as Suplementary Material). We observe good agreement between the experimental values and the CV model, as has been observed before for several saponins [6,34]. However, we observe higher values for the fitting parameters in our study.

In Golemanov et al. [34] the authors proposed an interpretation of the parameters in the CV model for *Quillaja* and *Yucca* saponins. They suggested that the relaxation of the Maxwell element, λ_0, is related to the sliding between densely packed domains or patches,

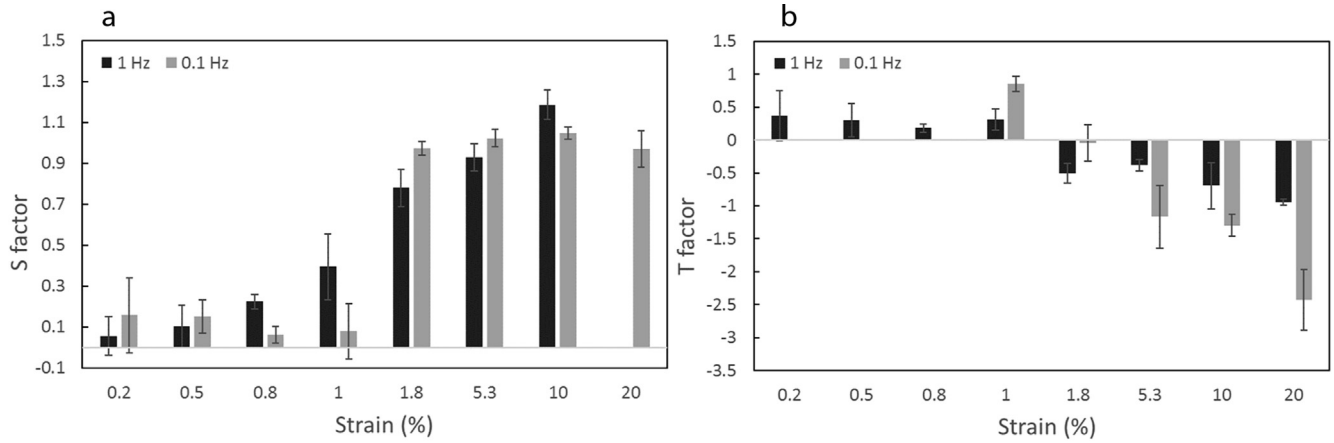

Fig. 8. S factor (a) and T factor (b) determined from strain sweeps of Escin, at frequencies of 0.1 Hz and 1 Hz. Measurements performed at 20 °C.

Table 2
CV model rheological parameters obtained from fitting Eqs. (4) and (5) simultaneously for the creep-recovery experiments

Parameter	
G_0 (N m^{-1})	1.09 ± 0.04
G_1 (N m^{-1})	3.21 ± 0.65
G_2 (N m^{-1})	8.09 ± 1.51
η_0 (N s m^{-1})	1844.48 ± 573.86
η_1 (N s m^{-1})	597.59 ± 97.51
η_2 (N s m^{-1})	110.20 ± 25.30
λ_0 (s)	1689.47 ± 495.36
λ_1 (s)	191.82 ± 40.07
$\lambda_2(s)$	14.15 ± 4.43

with weaker boundaries between them. Those weaker regions could in that view be the areas where fracture occurs. The relaxation of first and second kelvin elements (λ_1, λ_2) were suggested to be related to the reorganization of the molecules inside the domains to their preferred orientation, and the visco-plastic deformation in the domain boundaries, respectively. We observed similar λ_1 and λ_2 values to those found in [6]. The main difference between our relaxation times and those in [6] is λ_0, which is much longer in our case, resulting from the high viscosity of the Maxwell element (η_0).

As a first estimate, interfacial parameters can often be related to their 3D equivalents in the bulk phase by the scaling $B^s \sim Bh$, where B is the 3D equivalent of the surface parameter B^s, and h is the interfacial thickness. If we assume an interfacial layer thickness of 3 nm [6], the values for the interfacial rheological parameters correspond to a bulk shear modulus in the order of $\approx 10^8 - 0^9$ Pa which is similar to polyethylene and polycarbonate plastics. The surface shear viscosity corresponds to a bulk shear viscosity of $\approx 10^{10} - 10^{11}$ Pa s, which is in the same order of magnitude as cheddar cheese and asphaltic concrete [52]. These results show that Escin stabilized interfaces behave as a soft solid interface.

Although the interpretation of the creep results as proposed in [34], is not implausible, the emergence of multiple relaxation times does not always imply that there are multiple discrete relaxation processes of a different nature. In the relaxation of the step-dilatational deformations, we observed stretched exponential behavior, which is an indication of dynamic heterogeneity in the interfacial response. As a result of a distribution in 2D cluster size, we may have local variations in the relaxation kinetics, leading to a distribution of relaxation times [33]. For this reason, the recovery after creep was also fitted to a simple stretched exponential (Kohlrausch-Williams-Watts) function:

$$\gamma(t) = a\, exp^{(\frac{-\Delta t}{\tau_1})^{\beta}} + l \tag{6}$$

The β value we obtained again indicates dynamic heterogeneity in the response of the Escin-stabilized interface. Using a simple stretched exponential fit (Table 3), a β value between 0.41 and 0.48, which was similar to that seen for the relaxation after expansion. The relaxation time τ_1 is also of the same order of magnitude as in the step-dilatation experiment. So dynamic heterogeneity appears to be a plausible alternative explanation for the observed multi-exponential behavior.

4. Conclusion

Escin forms an interfacial structure of a disordered viscoelastic solid which, based on previous experiments for saponins [34], specifically for escin [6,7], and MD simulations for Escin [8,35], consist of 2D solid clusters. We extend the previous research within the LVE with new data beyond the linear regime. Studies of viscoelastic interfaces beyond the linear regime are still scarce in the literature [12,15,22–28] , even though in practice many deformations occur beyond the LVE regime. With the new data within the NLVE regime, the results from previous studies are confirmed, and new insight on the remarkable behavior of this interface in the NLVE regime is provided.

Using Lissajous plots to analyze LAOD deformations of Escin-stabilized air-water interfaces showed that these interfaces exhibit a highly non-linear behavior even at small deformations, and hence E'_d and E''_d obtained using the fundamental harmonic are clearly not very meaningful. In compression we observed significant strain softening, most likely due to the fact that after reaching a jammed state, 2D clusters start sliding over each other, leading to the formation of multilayers. Due to strong interactions within this structure no relaxation was observed after a sudden step-compression of the interface. Imaging with a high speed camera revealed that the formation of multilayers is preceded by transient

Table 3
Rheological parameters obtained from fitting a simple stretched exponential (Eq. (6)) for the recovery compliance after creep at different stresses. Creep was carried out for 150 s and recovery was monitored for 1000 s.

Parameter	0.209 mPa	0.52 mPa	1.5 mPa
β	0.48 ± 0.01	0.41 ± 0.04	0.41 ± 0.00
$\tau_1(s)$	6.83 ± 0.24	5.67 ± 0.47	4.5 ± 0.50

buckling of the interface, in which wrinkles appear, and these rapidly disappear again upon further compression. It is important to note, that at larger compression than the studied (10%), ejection of some of the clusters to the bulk cannot be discarded.

Recently, Sagis et al. [33] discussed the contributions of momentum transfer between the interface and bulk to the relaxation of viscoelastic interfaces, which is usually ignored in literature in favor of in-plane momentum transfer and mass transfer between the bulk and interface. In the relaxation after a step-expansion of the interface we observed dynamic heterogeneity, with a stretch exponent $\beta \approx 0.48$, indicating that momentum transfer between interface and bulk may also have a significant contribution to the relaxation behavior.

Surface LAOS measurements allowed for the characterization of this sytem as a 2D jammed system (and not a 2D gel), and the observation of fracture of the interfacial structure, visible as intra-cycle discontinuities in the Lissajous plots at strains around the crossover from solid to fluid-like behavior. The solid-like behavior with remarkably high interfacial shear elastic and viscous moduli was confirmed with creep-recovery experiments, and fitted to a Compound-Voigt model as used before [6,34]. In our work the recovery was also fitted with a stretched exponential functions again giving indication of a distribution of relaxation times [27,33,53], which results in $\beta \sim 0.41$–0.48, similar to the value observed in the step-expansion experiments.

Our LAOD and LAOS results, together with the analysis of relaxation using a stretched exponential function provide new insights on the structure of Escin-stabilized interfaces, and confirm earlier hypotheses on the origin of the extraordinarily high surface rheological parameters this component can impart on an interface. We believe these analyses shed also new light on previous studies performed on other saponin-stabilized interfaces with comparable highly elastic interfaces [37,45] as these might present similar interfacial layer structures, presenting dynamic heterogeneity.

Declaration of Competing Interest

The authors declare that they have no known competing financial interests or personal relationships that could have appeared to influence the work reported in this paper.

Appendix A. Supplementary material

Supplementary data associated with this article can be found, in the online version, at https://doi.org/10.1016/j.jcis.2019.12.053.

References

[1] Yang-Ping Niu, Lian-Da Li, Li-Mao Wu, Beta-aescin: a potent natural inhibitor of proliferation and inducer of apoptosis in human chronic myeloid leukemia K562 cells in vitro, Leukemia Lymphoma 49 (7) (2008) 1384–1391, https://doi.org/10.1080/10428190802090151.

[2] Emlia Hijová, Anna Chmelárová, Alojz Bomba, Effectiveness of bioactive food components in experimental colon carcinogenesis, Acta Veterinaria Brno 78 (4) (2009) 661–666, https://doi.org/10.2754/avb200978040661.

[3] Cesare R. Sirtori, Aescin: pharmacology, pharmacokinetics and therapeutic profile, Pharmacol. Res. 44 (3) (2001) 183–193, https://doi.org/10.1006/phrs.2001.0847.

[4] Tian Wang, Fenghua Fu, Leiming Zhang, Bin Han, Mei Zhu, Xiumei Zhang, Effects of escin on acute inflammation and the immune system in mice, Pharmacol. Rep. 61 (4) (2009) 697–704, https://doi.org/10.1016/S1734-1140(09)70122-7.

[5] Sandra Böttcher, Stephan Drusch, Saponins self-assembly and behavior at aqueous interfaces, Adv. Colloid Interface Sci. 243 (2017) 105–113, https://doi.org/10.1016/j.cis.2017.02.008.

[6] Konstantin Golemanov, Slavka Tcholakova, Nikolai Denkov, Edward Pelan, Simeon D. Stoyanov, Remarkably high surface visco-elasticity of adsorption layers of triterpenoid saponins, Soft Matter 9 (24) (2013) 5738, https://doi.org/10.1039/c3sm27950b.

[7] Nevena Pagureva, Slavka Tcholakova, Konstantin Golemanov, Nikolai Denkov, Eddie Pelan, Simeon D. Stoyanov, Surface properties of adsorption layers formed from triterpenoid and steroid saponins, Colloids Surf., A 491 (2016) 18–28, https://doi.org/10.1016/j.colsurfa.2015.12.001.

[8] Sonya Tsibranska, Anela Ivanova, Slavka Tcholakova, Nikolai Denkov, Self-assembly of Escin molecules at the AirWater interface as studied by molecular dynamics, Langmuir 33 (33) (2017) 8330–8341, https://doi.org/10.1021/acs.langmuir.7b01719.

[9] J. Lucassen, M. Van Den Tempel, Dynamic measurements of dilational properties of a liquid interface, Chem. Eng. Sci. 27 (6) (1972) 1283–1291, https://doi.org/10.1016/0009-2509(72)80104-0.

[10] J. Lucassen, M. Van Den Tempel, Longitudinal waves on visco-elastic surfaces, J. Colloid Interface Sci. 41 (3) (1972) 491–498, https://doi.org/10.1016/0021-9797(72)90373-6.

[11] Leonard M.C. Sagis, Peter Fischer, Nonlinear rheology of complex fluidfluid interfaces, Curr. Opin. Colloid Interface Sci. 19 (6) (2014) 520–529, https://doi.org/10.1016/j.cocis.2014.09.003.

[12] L.M.C. Sagis, K.N.P. Humblet-Hua, S.E.H.J. van Kempen, Nonlinear stress deformation behavior of interfaces stabilized by food-based ingredients, J. Phys.: Condens. Matter 26 (46) (2014) 464105, https://doi.org/10.1088/0953-8984/26/46/464105.

[13] F. Ravera, L. Liggieri, G. Loglio, Dilational rheology of adsorbed layers by oscillating drops and bubbles, in: Reinhard Miller, L. Liggieri (Eds.), Interfacial Rheology, one ed., CRC Press, Boca Raton, FL, USA, 2009, pp. 138–173 (chapter Five).

[14] A. Javadi, N. Mucic, M. Karbaschi, J.Y. Won, M. Lotfi, A. Dan, V. Ulaganathan, G. Gochev, A.V. Makievski, V.I. Kovalchuk, N.M. Kovalchuk, J. Krägel, R. Miller, Characterization methods for liquid interfacial layers, Eur. Phys. J. Spec. Top. 222 (1) (2013) 7–29, https://doi.org/10.1140/epjst/e2013-01822-3.

[15] Patrick A. Rühs, Christine Affolter, Erich J. Windhab, Peter Fischer, Shear and dilatational linear and nonlinear subphase controlled interfacial rheology of β-lactoglobulin fibrils and their derivatives, J. Rheol. 57 (3) (2013) 1003–1022, https://doi.org/10.1122/1.4802051.

[16] Randy H. Ewoldt, A.E. Hosoi, Gareth H. McKinley, New measures for characterizing nonlinear viscoelasticity in large amplitude oscillatory shear, J. Rheol. 52 (6) (2008) 1427–1458, https://doi.org/10.1122/1.2970095.

[17] Kyu Hyun, Sook Heun Kim, Kyung Hyun Ahn, Seung Jong Lee, Large amplitude oscillatory shear as a way to classify the complex fluids, J. Nonnewton. Fluid Mech. 107 (1–3) (2002) 51–65, https://doi.org/10.1016/S0377-0257(02)00141-6.

[18] Hani Hilles, Francisco Monroy, Laura J. Bonales, Francisco Ortega, Ramn G. Rubio, Fourier-transform rheology of polymer Langmuir monolayers: analysis of the non-linear and plastic behaviors, Adv. Colloid Interface Sci. 122 (1–3) (2006) 67–77, https://doi.org/10.1016/j.cis.2006.06.013.

[19] Hani Hilles, Armando Maestro, Francisco Monroy, Francisco Ortega, Ramn G. Rubio, Manuel G. Velarde, Polymer monolayers with a small viscoelastic linear regime: equilibrium and rheology of poly(octadecyl acrylate) and poly (vinyl stearate), J. Chem. Phys. 126 (12) (2007), https://doi.org/10.1063/1.2714514.

[20] Laura R. Arriaga, Ivn López-Montero, Ruddi Rodríguez-García, Francisco Monroy, Nonlinear dilational mechanics of Langmuir lipid monolayers: a lateral diffusion mechanism, Phys. Rev. E Stat. Nonlinear Soft Matter Phys. 77 (6) (2008) 1–10, https://doi.org/10.1103/PhysRevE.77.061918.

[21] Amelia Torcello-Gómez, Julia Maldonado-Valderrama, Mara J. Gálvez-Ruiz, Antonio Martín-Rodríguez, Miguel A. Cabrerizo-Vílchez, Juan De Vicente, Surface rheology of sorbitan tristearate and β-lactoglobulin: shear and dilatational behavior, J. Nonnewton. Fluid Mech. 166 (12–13) (2011) 713–722, https://doi.org/10.1016/j.jnnfm.2011.03.008.

[22] Silvia E.H.J. van Kempen, Henk A. Schols, Erik van der Linden, Leonard M.C. Sagis, Non-linear surface dilatational rheology as a tool for understanding microstructures of air/water interfaces stabilized by oligofructose fatty acid esters, Soft Matter 9 (40) (2013) 9579, https://doi.org/10.1039/c3sm51770e.

[23] Zhili Wan, Xiaoquan Yang, Leonard M.C. Sagis, Contribution of long fibrils and peptides to surface and foaming behavior of soy protein fibril system, Langmuir 32 (32) (2016) 8092–8101, https://doi.org/10.1021/acs.langmuir.6b01511.

[24] Zhili Wan, Xiaoquan Yang, Leonard M.C. Sagis, Nonlinear surface dilatational rheology and foaming behavior of protein and protein fibrillar aggregates in the presence of natural surfactant, Langmuir 32 (15) (2016) 3679–3690, https://doi.org/10.1021/acs.langmuir.6b00446.

[25] Anja Schröder, Claire Berton-Carabin, Paul Venema, Leonardo Cornacchia, Interfacial properties of whey protein and whey protein hydrolysates and their influence on O/W emulsion stability, Food Hydrocolloids 73 (2017) 129–140, https://doi.org/10.1016/j.foodhyd.2017.06.001.

[26] Marlies E.J. Geerts, Constantinos V. Nikiforidis, Atze Jan van der Goot, Albert van der Padt, Protein nativity explains emulsifying properties of aqueous extracted protein components from yellow pea, Food Struct. 14 (May) (2017) 104–111, https://doi.org/10.1016/j.foostr.2017.09.001.

[27] Jack Yang, Ilonka Thielen, Claire C. Berton-Carabin, Erik van der Linden, Leonard M.C. Sagis, Nonlinear interfacial rheology and atomic force microscopy of air-water interfaces stabilized by whey protein beads and their constituents, Food Hydrocolloids 101 (2020) 105466, https://doi.org/10.1016/j.foodhyd.2019.105466.

[28] Philipp Erni, Alan Parker, Nonlinear viscoelasticity and shear localization at complex fluid interfaces, Langmuir 28 (20) (2012) 7757–7767, https://doi.org/10.1021/la301023k.

[29] Ton van Vliet, Pieter Walstra, Large deformation and fracture behaviour of gels, Faraday Discuss. 101 (6) (1995) 359, https://doi.org/10.1039/fd9950100359.

[30] Ki Won Song, Hoa Youn Kuk, Gap Shik Chang, Rheology of concentrated xanthan gum solutions: oscillatory shear flow behavior, Korea Austr. Rheol. J. 18 (2) (2006) 67–81.
[31] Bao Wang, Li-jun Wang, Dong Li, Qing Wei, Benu Adhikari, The rheological behavior of native and high-pressure homogenized waxy maize starch pastes, Carbohydr. Polym. 88 (2) (2012) 481–489, https://doi.org/10.1016/j.carbpol.2011.12.028.
[32] H.S. Melito, C.R. Daubert, Rheological innovations for characterizing food material properties, Ann. Rev. Food Sci. Technol. 2 (1) (2011) 153–179, https://doi.org/10.1146/annurev-food-022510-133626.
[33] Leonard M.C. Sagis, Bingxue Liu, Yuan Li, Jeffrey Essers, Jack Yang, Ahmad Moghimikheirabadi, Emma Hinderink, Claire Berton-Carabin, Karin Schroen, Dynamic heterogeneity in complex interfaces of soft interface-dominated materials, Sci. Rep. 9 (1) (2019) 2938, https://doi.org/10.1038/s41598-019-39761-7.
[34] Konstantin Golemanov, Slavka Tcholakova, Nikolai Denkov, Edward Pelan, Simeon D. Stoyanov, Surface shear rheology of saponin adsorption layers, Langmuir 28 (33) (2012) 12071–12084, https://doi.org/10.1021/la302150j.
[35] Sonya Tsibranska, Anela Ivanova, Slavka Tcholakova, Nikolai Denkov, Structure of dense adsorption layers of Escin at the AirWater interface studied by molecular dynamics simulations, Langmuir 35 (39) (2019) 12876–12887, https://doi.org/10.1021/acs.langmuir.9b02260.
[36] Krassimir D. Danov, Rumyana D. Stanimirova, Peter A. Kralchevsky, Krastanka G. Marinova, Nikola A. Alexandrov, Simeon D. Stoyanov, Theodorus B.J. Blijdenstein, Eddie G. Pelan, Capillary meniscus dynamometry Method for determining the surface tension of drops and bubbles with isotropic and anisotropic surface stress distributions, J. Colloid Interface Sci. 440 (2015) 168–178, https://doi.org/10.1016/j.jcis.2014.10.067.
[37] R. Stanimirova, K. Marinova, Slavka Tcholakova, N.D. Denkov, S. Stoyanov, Edward Pelan, Surface rheology of saponin adsorption layers, Langmuir 27 (20) (2011) 12486–12498, https://doi.org/10.1021/la202860u.
[38] Matt Golding, Interfacial phenomena in structured foods, in: B. Bhandari, Y.H. Roos (Eds.), Food Materials Science and Engineering, vol. 8, Wiley-Blackwell, Oxford, UK, 2012, pp. 94–135. doi:10.1002/9781118373903.ch4. (Chapter 4).
[39] Sebastian Knoche, Dominic Vella, Elodie Aumaitre, Patrick Degen, Heinz Rehage, Pietro Cicuta, Jan Kierfeld, Elastometry of deflated capsules: elastic moduli from shape and wrinkle analysis, Langmuir 29 (40) (2013) 12463–12471, https://doi.org/10.1021/la402322g.
[40] T.B.J. Blijdenstein, P.W.N. de Groot, S.D. Stoyanov, On the link between foam coarsening and surface rheology: why hydrophobins are so different, Soft Matter 6 (8) (2010) 1799, https://doi.org/10.1039/b925648b.
[41] Philipp Erni, Hu.da.A. Jerri, Kenneth Wong, Alan Parker, Interfacial viscoelasticity controls buckling, wrinkling and arrest in emulsion drops undergoing mass transfer, Soft Matter 8 (26) (2012) 6958, https://doi.org/10.1039/c2sm25438g.
[42] Paulo Hoyer, Vladimir Alvarado, Stability of liquid bridges with elastic interface, RSC Adv. 7 (78) (2017) 49344–49352, https://doi.org/10.1039/C7RA09657G.
[43] Yu-Jiun Lin, Sourav Barman, Peng He, Zhuqing Zhang, Gordon F. Christopher, Sibani Lisa Biswal, Combined interfacial shear rheology and microstructure visualization of asphaltenes at air-water and oil-water interfaces, J. Rheol. 62 (1) (2018) 1–10, https://doi.org/10.1122/1.5009188.
[44] Chun-Xia Zhao, Erik Miller, Justin J. Cooper-White, Anton P.J. Middelberg, Effects of fluid-fluid interfacial elasticity on droplet formation in microfluidic devices, AIChE J. 57 (7) (2011) 1669–1677, https://doi.org/10.1002/aic.12382.
[45] Kamil Wojciechowski, Surface activity of saponin from Quillaja bark at the air/water and oil/water interfaces, Colloids Surf., B 108: 95–102 (2013) 8, https://doi.org/10.1016/j.colsurfb.2013.02.008.
[46] Pietro Cicuta, Compression and shear surface rheology in spread layers of β-casein and β-lactoglobulin, J. Colloid Interface Sci. 308 (1) (2007) 93–99, https://doi.org/10.1016/j.jcis.2006.12.056.
[47] M.R.B. Mermet-Guyennet, J. Gianfelice de Castro, M. Habibi, N. Martzel, M.M. Denn, D. Bonn, LAOS: the strain softening/strain hardening paradox, J. Rheol. 59 (1) (2015) 21–32, https://doi.org/10.1122/1.4902000.
[48] Simon A. Rogers, Brian M. Erwin, Dimitris Vlassopoulos, Michel Cloitre, A sequence of physical processes determined and quantified in LAOS: application to a yield stress fluid, J. Rheol. 55 (2) (2011) 435–458, https://doi.org/10.1122/1.3544591.
[49] Juntae Kim, Dimitri Merger, Manfred Wilhelm, Matthew E. Helgeson, Microstructure and nonlinear signatures of yielding in a heterogeneous colloidal gel under large amplitude oscillatory shear, J. Rheol. 58 (5) (2014) 1359–1390, https://doi.org/10.1122/1.4882019.
[50] Fabian C. Birbaum, Sanna Haavisto, Antti Koponen, Erich J. Windhab, Peter Fischer, Shear localisation in interfacial particle layers and its influence on Lissajous-plots, Rheol. Acta 55 (4) (2016) 267–278, https://doi.org/10.1007/s00397-016-0912-0.
[51] Suthsiri Precha-Atsawanan, Dudsadee Uttapap, Leonard M.C. Sagis, Linear and nonlinear rheological behavior of native and debranched waxy rice starch gels, Food Hydrocolloids 85 (March) (2018) 1–9, https://doi.org/10.1016/j.foodhyd.2018.06.050.
[52] Howard A. Barnes, A Handbook Of Elementary Rheology, Cambrian Printers, Aberyswyth, first ed., 2000.
[53] J. Klafter, M.F. Shlesinger, On the relationship among three theories of relaxation in disordered systems, Proc. Nat. Acad. Sci. 83 (4) (1986) 848–851, https://doi.org/10.1073/pnas.83.4.848.